Received: 31 July 2020 | Revised: 16 December 2020 | Accepted: 11 January 2021

DOI: 10.1002/hbm.25350

RESEARCH ARTICLE

WILEY

Network interdigitations of Tau and amyloid-beta deposits define cognitive levels in aging

Chan-Mi Kim[1,2] | Victor Montal[1,3,4] | Ibai Diez[1,2] | William Orwig[1,2] | Alzheimer's Disease Neuroimaging Initiative (ADNI) | Jorge Sepulcre[1,2]

[1]Gordon Center for Medical Imaging, Department of Radiology, Massachusetts General Hospital, Harvard Medical School, Boston, Massachusetts

[2]Athinoula A. Martinos Center for Biomedical Imaging, Department of Radiology, Massachusetts General Hospital, Harvard Medical School, Charlestown, Massachusetts

[3]Memory Unit, Department of Neurology, Hospital de la Santa Creu i Sant Pau, Biomedical Research Institute Sant Pau, Universitat Autonoma de Barcelona, Barcelona, Spain

[4]Centro de Investigacón Biomédica en Red de Enfermedades Neurodegenerativas (CIBERNED), Spain

Correspondence
Jorge Sepulcre, Gordon Center for Medical Imaging, Department of Radiology, Massachusetts General Hospital, Harvard Medical School, 13th Street, Charlestown, MA 02129.
Email: sepulcre@nmr.mgh.harvard.edu, jsepulcre-bernad@mgh.harvard.edu

Funding information
National Institute on Aging, Grant/Award Numbers: R01AG061445, R01AG061811

Abstract

Amyloid-beta (Aβ) plaques and tau neurofibrillary tangles are pathological hallmarks of Alzheimer's disease (AD); their contribution to neurodegeneration and clinical manifestations are critical in understanding preclinical AD. At present, the mechanisms related to Aβ and tau pathogenesis leading to cognitive decline in older adults remain largely unknown. Here, we examined graph theory-based positron emission tomography (PET) analytical approaches, within and between tau and Aβ PET modalities, and tested the effects on cognitive changes in cognitively normal older adults (CN). Particularly, we focused on the network interdigitations of Aβ and tau deposits, along with cognitive test scores in CN at both baseline and 2-year follow-up (FU). We found highly significant Aβ-tau network integrations in AD vulnerable areas, as well as significant associations between those Aβ-tau interdigitations and general cognitive impairment in CN at baseline and FU. Our findings suggest a distinctive contribution of interlinking network relationships between Aβ and tau deposits in heteromodal areas of the human brain. They support a network-based interaction between Aβ and tau accumulations as a key factor for cognitive deterioration in CN prior to dementia.

KEYWORDS
aging, Alzheimer's disease, amyloid PET, cognition, connectivity analysis, Tau PET

1 | INTRODUCTION

Alzheimer's disease (AD) is the most common type of dementia characterized by progressive memory loss and the loss of independence in daily activities. Aggregation of amyloid-beta (Aβ) peptides and accumulation of aggregated forms of tau proteins are pathological hallmarks of AD, appearing in initial stages of AD prior to onset of symptoms (Fleisher et al., 2015; Jack Jr et al., 2010; Jansen et al., 2015). Two pathological hallmarks, Aβ plaques and the neurofibrillary tangles, are considered sensitive markers for AD, and their contribution to neurodegeneration and cognitive decline is presumed to be a key to understand preclinical AD (Ballard et al., 2011; Johnson et al., 2013; Pike et al., 2007). However, at present, it remains largely unknown how Aβ and tau accumulation spatially intersect in brain circuits and whether these factors may explain the emergence of cognitive decline in older adults.

Increased Aβ plaques and tau neurofibrillary tangles are commonly found in the neocortex of AD patients in postmortem autopsies (Braak & Braak, 1991a, 1991b, 1995) as well as in positron emission tomography (PET) imaging studies (Barthel et al., 2011; Chien

et al., 2013; Clark et al., 2011; Clark et al., 2012; Johnson et al., 2016; Klunk et al., 2004; Marquié et al., 2015; Pike et al., 2007; Vandenberghe et al., 2010; Wong et al., 2010). The coexistence of both pathological hallmarks is associated with synaptic dysfunction and neuronal loss that mediate memory and cognition (Iqbal & Grundke-Iqbal, 2002; Selkoe, 2002; Sperling et al., 2019). Several studies have shown a strong association between Aβ and greater tau accumulations at the cellular and molecular levels (Bennett et al., 2017; Götz, Chen, Van Dorpe, & Nitsch, 2001; He et al., 2018; Hurtado et al., 2010; Lewis et al., 2001; Williamson, Usardi, Hanger, & Anderton, 2008). The spatial association between Aβ and tau accumulations is somewhat inconsistent or minimally overlapping in specific regions of the brain in older adults prior to dementia (Schöll et al., 2016; Whitwell et al., 2018). Aβ plaques first arise in the neocortex and spread to deep subcortical regions, while tau neurofibrillary tangles occur in entorhinal and limbic areas first, then spread to the neocortical areas (Arnold, Hyman, Flory, Damasio, & Van Hoesen, 1991; Braak & Braak, 1991b, 1995). Thus, the lack of spatial consistency between Aβ and tau accumulations has resulted from the distinctive spreading patterns of Aβ pathology and tau pathology in AD progression (Arnold et al., 1991; Braak & Braak, 1991b, 1995). Although there is not a perfect alignment of spatial distributions, a potential contribution of global Aβ accumulation to increasing accumulation of tau was suggested by several imaging studies (Jacobs et al., 2018; Pontecorvo et al., 2017; Quiroz et al., 2018; Wang et al., 2016), particularly if distributed network information is taken into consideration. In fact, it is now known that regions of Aβ and tau accumulation show network bonds, even without spatial overlapping between them (Brier et al., 2016;Iaccarino et al., 2018; Sepulcre et al., 2016). Therefore, understanding the spatial and network interactions between Aβ and tau accumulations in cognitively healthy participants may elucidate the underlying role of both pathologies in the development of cognitive decline.

Given the increasing evidence of the transcellular propagation of AD pathogenesis along neuronal circuits as well as in functionally linked distributed regions (Braak & Del Tredici, 2011; Clavaguera et al., 2009; De Calignon et al., 2012; Guo & Lee, 2014; Iba et al., 2013; Stöhr et al., 2012; Thal, Rub, Orantes, & Braak, 2002; Walker & Jucker, 2011), graph theory-based network approaches have been applied to understand how Aβ and tau propagate in the in vivo human brain (Kim et al., 2019; Sepulcre et al., 2016; Sepulcre et al., 2018). The network-based spatial spreading patterns of Aβ and tau accumulations have shown distinctive pathways, such as tau propagation from medial/inferior temporal lobe to orbitofrontal cortex, and Aβ propagation from posterior cingulate cortex (PCC) to lateral parietal lobe, in older adults (Sepulcre et al., 2016), mild AD (Iaccarino et al., 2018), and AD spectrum patients (Kim et al., 2019). However, some hubs of both Aβ and tau pathology networks overlapped in regions which are partly associated with AD vulnerability (Iaccarino et al., 2018; Kim et al., 2019; Sepulcre et al., 2016; Sepulcre et al., 2018). Additionally, local tau accumulation was significantly associated with distributed Aβ accumulation, which suggested a potential network dependency between Aβ and tau accumulations in older adults or mild AD (Iaccarino et al., 2018; Sepulcre et al., 2016).

Previously, a strong association between the spatial distribution of tau accumulation and cognitive impairment was observed, primarily in the medial temporal lobe (MTL), in older adults and AD (Ghoshal et al., 2002; Mitchell et al., 2002; Nelson et al., 2012; Quiroz et al., 2018; Rolstad et al., 2013; van Rossum et al., 2012). Although tau is more closely associated with cognitive impairment than Aβ (Ghoshal et al., 2002; Mitchell et al., 2002; Nelson et al., 2012; Quiroz et al., 2018; Rolstad et al., 2013; van Rossum et al., 2012), a significant association between the longitudinal trajectories of Aβ and the progressive cognitive decline, particularly memory function, has been also observed in aging or in the early stages of AD (Hanseeuw et al., 2019; Landau et al., 2012; Resnick et al., 2010; Villemagne et al., 2013). Other studies have suggested that neocortical Aβ accumulation potentially contributes to the association of tau with cognitive impairment in older adults (Hanseeuw et al., 2019; Jacobs et al., 2018; Schöll et al., 2016; Sperling et al., 2019) and early stages of AD (Fagan et al., 2007; Johnson et al., 2016). However, the mechanism of the association between Aβ and tau pathogenesis that links to cognitive decline in older adults prior to AD remains largely unknown.

Given that the network physical dependencies and overlapping distributions of Aβ and tau in the neocortex -also called Aβ-tau interdigitations in this study- have been suggested recently (Kim et al., 2019; Sepulcre et al., 2016; Sepulcre et al., 2018), it is critical to examine whether Aβ accumulation and tau accumulation affect subtle cognitive impairment independently, or combination of Aβ and tau accumulations have synergetic effects in older adults with clinically normal cognition prior to symptom onset. To date, little is known about the role of the association between Aβ and tau accumulations in longitudinal cognitive changes in aging. Therefore, investigating the network-based PET correlation between Aβ and tau deposits, and their association with the cognitive variability in older adults may provide insights into how preclinical AD progresses into a more patent cognitive failure.

In this study, we explore the network-based relationships between Aβ and tau accumulations in cognitively healthy older adults measured by PET images. Next, we examine the association between PET network profiles and neuropsychological (NP) test scores in order to understand the effects of the Aβ and tau network relationships at baseline and 2-year follow-up (FU). Our findings support the distinctive contribution of Aβ-tau pathological connectivity crosstalk in the appearance of the initial cognitive changes in putative preclinical stages of AD in older adults.

2 | MATERIALS AND METHODS

2.1 | Participants

A total of 193 cognitively normal older adults (CN) from Alzheimer's Disease Neuroimaging Initiative (ADNI) projects (http://www.loni.

ucla.edu/ADNI/) who completed cognitive assessment, T1-weighted magnetic resonance imaging (MRI), 18F-Florbetapir (FBP) PET, and 18F-AV-1451 (tau) PET at baseline visits were investigated. We excluded nine subjects due to technical limitations of image processing, such as a failure of coregistration between T1-MRI and PET or the failure of the partial volume correction (PVC) process in PET images. All data used in this study was acquired from ADNI-3 project between August 2016 and December 2019 (Weiner et al., 2017). Cognitive assessment was performed using NP tests, such as Clinical Dementia Rating, Mini Mental State Examination (MMSE) (Folstein, Folstein, & McHugh, 1975), Geriatric Depression Scale, Rey Auditory Verbal Learning Test (RAVALT) (Rey, 1958), Alzheimer's Disease Assessment Scale-Cognitive Subscale (ADAS-Cog) (Mohs et al., 1997a, 1997b), ADNI composite score for memory (ADNI-MEM) (Crane et al., 2012), and ADNI composite score for executive function (ADNI-EF) (Gibbons et al., 2012). We additionally investigated the FU data in twenty CN, who completed the cognitive assessment, T1-weighted MRI, FBP PET and tau PET at the 2-year FU time point, for the validation analysis in this study. Two FU data were excluded due to the failure of the PET-preprocessing. Finally, we defined three groups of CN, with 184 CN at baseline, 18 CN at 2-year FU, and FU-matched 18 CN at baseline, for the longitudinal analysis. FU-matched CN at baseline was subselected from all CN at baseline. Detailed demographic characteristics and NP test scores of all participants are described in Table 1.

2.2 | MRI acquisition

T1-weighted MRIs were acquired using an accelerated sagittal magnetization-prepared rapid gradient echo sequence on 3-T SIEMENS systems (repetition time = 2.3 ms, echo time = 2.9 ms, flip angle = 9.0°, image matrix = 256 × 256, 210 slices, voxel size = 1.0 × 1.0 mm, slice thickness = 1.0 mm) or on 3-T Phillips Systems (repetition time = 6.5 ms, echo time = 2.9 ms, flip angle = 9.0°, image matrix = 256 × 256, 210 slices, voxel size = 1.0 × 1.0 mm, slice thickness = 1.0 mm). Some T1-weighted MRIs were acquired using an accelerated sagittal inversion recovery-prepared fast spoiled gradient-echo sequence on 3-T GE systems (repetition time = 7.7 ms, echo time = 3.1 ms, flip angle = 11.0°, image matrix = 256 × 256, 196 slices, voxel size = 1.0 × 1.0 mm, slice thickness = 1.0 mm). Detailed information of the MRI acquisition protocol is available from ADNI website (http://www.loni.ucla.edu/ADNI/).

2.3 | PET acquisition

FBP (Aβ) PET scan was performed for 20 min in duration by 4-by-5 min frames and was acquired starting 50–70 min after injection of 10.0 ± 1.0 mCi F18-Florbetapir. Tau PET scan was performed for 30 min in duration by 6-by-5 min frames and was acquired starting 75–105 min after injection of 10.0 ± 1.0 mCi F18-AV-1451. Both FBP PET and tau PET images were acquired using one of several PET scanners, including GE, Siemens, or Phillips Medical Systems. The detailed methods for FBP PET and tau PET acquisitions are described elsewhere (Weiner et al., 2017). We used an averaged single FBP PET and the averaged single tau PET from ADNI database, which were generated by averaging all frames of FBP PET or tau PET image set. All PET images were reconstructed with 1.02 × 1.02 mm pixel size and 2.0 mm slice thickness; or 1.33 × 1.33 mm pixel size and 3.27 mm slice thickness; or 2.0 × 2.0 mm pixel size and 3.27 mm slice thickness depending on their scanner types. Detailed PET acquisition information is available from ADNI website (http://www.loni.ucla.edu/ADNI/).

TABLE 1 Demographics and clinical characteristics

	CN at baseline (*n* = 184)	FU-matched CN at baseline (*n* = 18)	CN at 2-year FU (*n* = 18)
Gender	F = 106/M = 78	F = 11/M = 7	F = 11/M = 7
Age (years)	74.92 ± 9.50	77.13 ± 6.31	79.22 ± 7.22
Education (years)	16.25 ± 3.44	15.30 ± 4.32	15.30 ± 4.32
MMSE	28.80 ± 2.51	29.06 ± 1.21	28.40 ± 1.64
CDR (IQR)	0.04 (0.0–0.0)	0.11 (0.0–0.0)	0.25 (0.0–0.5)
MoCA	24.73 ± 3.41	24.72 ± 3.20	23.35 ± 3.25
GDS	0.92 ± 1.57	0.89 ± 1.49	1.35 ± 1.87
RAVALT	45.24 ± 10.63	44.00 ± 8.22	36.00 ± 14.59
ADAS-Cog	12.97 ± 5.22	13.04 ± 4.40	13.53 ± 6.35
ADNI-MEM	0.93 ± 0.56	0.83 ± 0.40	0.66 ± 0.86
ADNI-EF	1.02 ± 0.79	1.18 ± 0.80	0.92 ± 0.74
Amyloid positivity (global FBP-SUVR ≥ 1.10)	30.77%	44.44%	
tau positivity (composite ROIs ≥ 1.25)	2.73%	5.56%	

Abbreviations: ADAS-Cog, Alzheimer's Disease Assessment Scale-Cognitive Subscale; ADNI-EF, Alzheimer's Disease Neuroimaging Initiative composite score for executive function; ADNI-MEM, Alzheimer's Disease Neuroimaging Initiative composite score for memory; CDR, Clinical Dementia Rating; CN, cognitively normal older adults; FBP, 18F-Florbetapir; FU, follow-up; GDS, Geriatric Depression Scale; IQR, interquartile range; MMSE, Mini Mental State Examination; MoCA, Montreal Cognitive Assessment; RAVALT, Rey Auditory Verbal Learning Test; SUVR, standardized uptake value ratio.

2.4 | MRI image processing

All T1-weighted MRIs at baseline and 2-year FU were automatically processed by FreeSurfer recon-all procedure (FreeSurfer version 6.0.0; http://surfer.nmr.mgh.harvard.edu/) to reconstruct cortical surfaces and to segment region-of-interests (ROI) volumes (Dale, Fischl, & Sereno, 1999; Desikan et al., 2006; Fischl, Sereno, Tootell, & Dale, 1999). The ROI volumes were defined by the gyral-based Desikan–Killiany atlas through an automated FreeSurfer process, which used the depth from one sulcus to another to parcellate the cerebral cortex into standard neuroanatomical regions, for each individual MRI (Desikan et al., 2006). All technical details of these procedures are described in prior publications (Dale et al., 1999; Desikan et al., 2006; Fischl et al., 2002; Fischl, van der Kouwe, et al., 2004; Fischl, Salat, et al., 2004; Fischl, Liu, & Dale, 2001). The brain tissues, including gray matter (GM), white matter (WM), and cerebrospinal fluid, were segmented from T1-weighted MRI and volume registered into Montreal Neurological Institute/International Consortium for Brain Mapping (MNI/ICBM) space using watershed/surface deformation procedure (Ségonne et al., 2004). The registered MRIs automatically mapped into a common surface template using a surface-based averaging technique by considering cortical folding patterns. Then, predefined ROIs in the standard space were inversely mapped to each native MRI using a high-dimensional spherical morphing procedure to segment the ROIs in each individual (Fischl et al., 2002; Fischl, Salat, et al., 2004; Fischl, van der Kouwe, et al., 2004). In order to calculate the standard uptake value ratio (SUVR) and to perform the PVC in PET image processing, we used ROIs to define the reference regions of PET images for each individual.

2.5 | PET image processing

All FBP PET and tau PET at both baseline and 2-year FU were processed by FMRIB Software Library (FSL; http://fsl.fmrib.ox.ac.uk) and FreeSurfer PetSurfer procedure (FreeSurfer version 6.0.0; http://surfer.nmr.mgh.harvard.edu/fswikiPetSurfer/) to perform coregistration, calculation of SUVR, and to perform PVC (Greve et al., 2016). Each individual FBP PET or tau PET image was coregistered to the corresponding native T1-weighted MRI using a rigid-body registration with mutual information cost function. All ROIs that segmented from individual MRI were inversely registered to each individual FBP PET or tau PET by using an inverse transformation of each coregistration matrix. Then, each individual FBP PET or tau PET was scaled by a mean value in the cerebellar gray reference region to calculate the SUVR (Sepulcre et al., 2018). To examine the pathological status of our population, we additionally investigated amyloid-positivity and tau-positivity in CN at baseline. The amyloid-positivity was defined by considering the recommended threshold of global FBP-SUVR ≥1.10 in each individual (Joshi et al., 2012). The global FBP-SUVR was calculated as the ratio of the mean FBP-SUVR of six cortical ROIs, including frontal, temporal, precuneus, parietal, anterior cingulate, and posterior cingulate cortices, to whole cerebellum reference region without performing PVC. The tau-positivity was defined by using the tau cut-off threshold of composite ROIs ≥1.25 in each individual (Mishra et al., 2017). The mean tau-SUVR in the composite ROIs, including the entorhinal, lateral occipital, inferior temporal cortices and amygdala, was divided by a mean value in the cerebellar gray reference region to decide tau-positivity in CN at baseline (Mishra et al., 2017). Individual FBP-SUVR and tau-SUVR images were corrected for partial volume effects by using an extended Müller–Gärtner (MG) method, which estimates a true radioactivity concentration in human brain GM by considering a heterogeneity of GM activity via four-compartment model, within PetSurfer procedure (Meltzer et al., 1996; Muller-Gartner et al., 1992; Rousset, Ma, & Evans, 1998). A GM threshold for PVC was set at 0.1 and the point spread function for PVC was estimated at 8 mm. Detailed methodological explanation of MG PVC is described in a prior publication (Greve et al., 2016). After that, individual partial volume corrected FBP-SUVR and tau-SUVR images were coregistered to the corresponding MRI and then registered to MNI/ICBM template by using the transformation matrixes obtained from the previous step. All partial volume corrected PET data were down sampled from the standard space to 6 mm isovoxel to avoid computational limitations of the high-dimensional data. We used 6 mm isotropic MNI/ICBM template to define the structural information in all PET data.

2.6 | Group averaged FBP-SUVR and tau-SUVR

To examine overall distributed patterns of both Aβ deposition and tau deposition in CN, the group averaged FBP-SUVR map and tau-SUVR map at baseline and 2-year FU were calculated in voxel-based MNI space. Then, the voxel-based group averaged PET-SUVR maps were mapped into an averaged cortical surface by mapping a value of the middle point between inner and outer surfaces in each vertex point via FreeSurfer recon-all procedure (FreeSurfer version 6.0.0; http://surfer.nmr.mgh.harvard.edu/). Longitudinal changes in FBP-SUVR and tau-SUVR between CN at 2-year FU and FU-matched baseline were investigated using a paired *t*-test in each voxel, and then mapped into an averaged cortical surface via FreeSurfer recon-all procedure (FreeSurfer version 6.0.0; http://surfer.nmr.mgh.harvard.edu/). To determine significant change, false discovery rate (FDR) set at $q < 0.05$ was performed for multiple comparisons (Benjamini & Hochberg, 1995).

2.7 | Graph theory-based PET correlation within single PET modality and between PET modalities

We measured voxel-level correlations within single PET modality and different PET modalities. We created graph theory-based correlation matrices, which defined a node as a voxel in GM and an edge as a partial correlation coefficient between a pair of voxels of PET SUVR data

in GM across all CN. To remove confounding effects, we adjusted all partial correlations by age, sex, as well as the PET-SUVR values of the PET modality not included in that specific analysis (see details in the following sections). All voxel-based partial correlations were calculated by Statistics and Machine Learning Toolbox within MATLAB.

2.7.1 | Partial PET correlation within single PET modality

Each Aβ-to-Aβ correlation between different voxels was measured by the partial correlation between a FBP-SUVR in a start voxel *b* and a FBP-SUVR in the paired voxel *d* across all possible pairs of voxels within GM in CN while controlling for age, sex, and tau-SUVR in the paired voxel *d*. Similarly, each Tau-to-Tau correlation was measured by the partial correlation between a tau-SUVR in a start voxel *b* and a tau-SUVR in the paired voxel *d* across all possible pairs of voxels within GM in CN while controlling for age, sex, and FBP-SUVR in the paired voxel *d*. We obtained 6,848-by-6,848 matrix $D_{withinPET}$ in each correlation within single PET modality in group level. To determine significant correlation, we corrected for multiple comparisons in each correlation matrix $D_{withinPET}$ by using a FDR set at $q < 0.05$ (Benjamini & Hochberg, 1995).

2.7.2 | Partial PET correlation between different PET modalities

Each Aβ-to-Tau correlation between different voxels was measured by the partial correlation between a FBP-SUVR in a start voxel *b* and a tau-SUVR in the paired voxel *d* across all possible pairs of voxels within GM in CN while controlling for age, sex, and FBP-SUVR in the paired voxel *d* (Figure 1a). Each Tau-to-Aβ correlation was measured by the partial correlation between a tau-SUVR in a start voxel *b* and a FBP-SUVR in the paired voxel *d* across all possible pairs of voxels within GM in CN while controlling for age, sex, and tau-SUVR in the paired voxel *d* (Figure 1a). We obtained 6,848-by-6,848 matrix $D_{betweenPET}$ in each correlation between different PET modalities in group level. The FDR correction was performed at *q* as 0.05 in each correlation matrix $D_{betweenPET}$ to determine the significant correlation (Benjamini & Hochberg, 1995).

2.7.3 | Weighted degree of the correlation matrix

We calculated the weighted degree (WD) of each voxel in each correlation matrix *D* to identify which voxel's PET-SUVR were highly correlated with PET-SUVRs of the rest of GM voxels. The WD of a voxel *b* was calculated as the sum of the significant correlation coefficients between voxel *b* and all possible paired voxel *d*, excluding a self-connection. High WD in voxel *b* indicates that the PET-SUVR of the voxel *b* have significantly large number of correlations to the rest of paired-voxels in comparison with other voxels. Thus, a voxel with high WD can be described as a hub voxel, which is strongly correlated with the rest of the paired-voxels. The WD of all 6,848 voxels was calculated in each correlation matrix *D* and then resampled to the corresponding GM voxels in the MNI template. Finally, we obtained the WD map of Aβ-to-Aβ, Tau-to-Tau, Aβ-to-Tau, and Tau-to-Aβ correlation matrixes in group level at baseline.

2.8 | Relationship between the information of the graph theory-based correlation matrix and cognitive variability

Flowchart for identifying the relationship between the averaged PET-SUVR and cognitive variability in the PET correlation between different PET modalities is shown in Figure 1. We examined correlation between averaged PET-SUVRs of each paired-voxels and cognitive scores in each PET-to-PET correlation combination. The linear association analysis was performed to determine whether the information of the graph theory-based PET correlations is associated with cognitive variability or not, as well as to identify which PET correlation, such as the correlation within single PET modality or the PET correlation between different PET modalities, is better associated with the cognitive variability in CN. First, we calculated the averaged PET-SUVR between a start voxel and the paired voxel, which was defined by a significant correlation in the PET correlation matrix *D*, across all possible voxel pairs in each correlation matrix *D*, in each individual level at baseline. Next, we investigated relationships between the averaged PET-SUVR and NP scores, including MMSE, RAVALT, ADAS-Cog, ADNI-MEM, and ADNI-EF, in each type of PET correlation matrix in CN at baseline by using Pearson's partial correlation analysis. Third, we constructed a linear plot between the averaged PET-SUVR in each paired-voxels and each NP score to examine a linear trend between the averaged PET-SUVR in each paired-voxels and each NP score in CN at baseline (Figure 1b).

Our correlation approach between PET-SUVRs and NP scores is sensitive to detect direct association between the network profiles of Aβ and tau accumulation and the cognitive scores of our samples. Thus, they indicate whether a voxel displays an overall significant association between network pathology and cognitive variability. However, these correlations values do not provide information about how initial or late are these associations along the pathological process. To obtain this additional information, we used a centroid-based strategy. We calculated the centroid values of voxel-level correlations in order to determinate whether an Aβ, tau and NP correlation was predominantly populated by values in specific areas of the dispersion graph. For instance, a low centroid value would reflect a combination of low pathology and normal cognition (or initial states), while a high centroid value would reflect a combination of high pathology and impaired cognition (late states) (Figure 1b). We calculated centroid values of the cognition-related

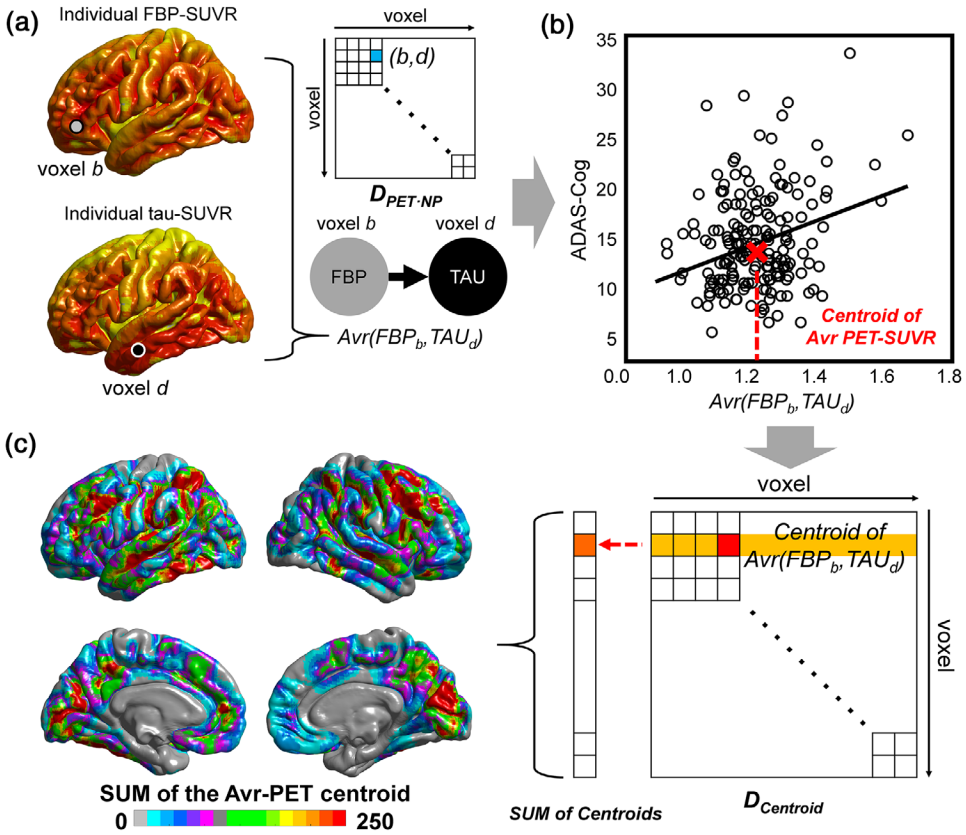

FIGURE 1 Flowchart for measurement of sum of centroid values of averaged positron emission tomography (PET)-SUVR between different modalities by using PET-to-NP correlation. (a) An averaged PET-SUVR (Avr(FBP_b,tau_d)) was calculated by averaging between FBP-SUVR of a voxel *b* (FBP_b) and tau-SUVR of the paired voxel *d* (tau_d) that is significantly associated with the voxel *b* in FBP-to-Tau correlation matrix ($D_{betweenPET}$) (FDR corrected $q < 0.05$) across all CN at baseline and 2-year FU. Then, PET-to-NP correlation matrix was calculated by Pearson's partial correlation between the averaged PET-SUVR (Avr(FBP_b,tau_d)) and ADAS-Cog scores while controlling for age, sex, years of education in CN at baseline only (FDR corrected $q < 0.05$). (b) A centroid of the averaged PET-SUVRs was calculated by considering the scattered plots between the averaged PET-SUVRs of each paired voxels (*b*,*d*) and ADAS-Cog scores. The centroid value was only calculated if the FBP-SUVR was significantly correlated with tau-SUVR in the corresponding link between voxel *b* and voxel *d* from the FBP-to-Tau correlation matrix (FDR corrected $q < 0.05$). (c) A sum of the centroid values in each voxel was calculated by summation of the centroid values across all possible correlations between the voxel *b* and the rest of the gray matter voxels from the centroid matrix to make a spatial map of the cognition-related PET uptakes in different PET modalities. The map of the sum of the centroid values was calculated in CN at baseline. Red color of (a) indicates high PET uptakes. Black circle of (b) indicates each individual in CN at baseline and red cross marker of (b) indicates the centroid of the averaged PET-SUVRs in plot distribution. Color bar of (c) indicates the sum of the centroid values in CN at baseline. ADAS-Cog, Alzheimer's Disease Assessment Scale-Cognitive Subscale; Avr, averaged; CN, cognitively normal older adults; FBP, 18F-Florbetapir; FDR, false discovery rate; NP, neuropsychological; SUVR, standardized uptake value ratio; tau, F18-AV-1451

averaged PET-SUVRs and then made centroid maps using the CN sample at baseline (Figure 1b,c). We only calculated the centroid if the averaged PET-SUVRs in each paired-voxels was significantly correlated with NP score. Next, we made spatial maps of the centroid by summation of the centroid values across all possible connections related to each voxel in group level to visualize the effects of the graph theory-based single PET uptakes or multimodal PET uptakes in cognitive variability in CN at baseline. The centroid map was used to examine whether the centroid value of the graph theory-based PET uptake is reliably and constantly associated with the NP test scores in CN at both baseline and FU point for further validation analysis.

2.8.1 | Measurement of averaged PET-SUVR

We calculated the averaged PET-SUVR between a PET-SUVR of a start voxel and a PET-SUVR of the paired voxel, which had a significant correlation in the PET correlation matrix *D* after performing FDR correction, in each PET correlation matrix *D* (Figure 1a, left side and right bottom). The averaged PET-SUVR between a PET-SUVR of a start voxel *b* (PET_b) and a PET-SUVR of the paired voxel *d* (PET_d) that linked by *i*th edge (E_i) of each PET correlation matrix *D* in each subject *k* was defined as follows:

$$\mu_k^D(i) = Avr(PET_b, PET_d) | E_i \text{ of matrix } D \,(\text{FDR corrected } q < 0.05)$$

According to this equation, We obtained four types of the averaged PET-SUVRs (μ), such as $Avr(FBP_b, FBP_d)$, $Avr(TAU_b, TAU_d)$, $Avr(FBP_b, TAU_d)$, and $Avr(TAU_b, FBP_d)$, across all CN at baseline by considering each type of PET correlation matrix D. Finally, we obtained 6,848-by-6,848 matrix, which consisted of the averaged PET-SUVRs, in each type of PET correlation matrix D in each individual. All averaged PET-SUVRs were adjusted for age and sex via a general regression model by Statistics and Machine Learning Toolbox within MATLAB.

2.8.2 | Partial correlation between the averaged PET-SUVRs and cognitive scores

The correlations between the averaged PET-SUVRs in each paired-voxels and NP scores, including MMSE, RAVALT, ADAS-Cog, ADNI-MEM, and ADNI-EF, were performed by partial correlation analysis in each type of PET correlation matrix D in CN at baseline. We constructed four types of 6,848-by-6,848 correlation matrices $D_{PET\cdot NP}$, which consisted of the correlation coefficients between the averaged PET-SUVRs and each NP score in group level (Figure 1a, right upper matrix). All correlations between the averaged PET-SUVRs and NP scores were in each correlation matrix $D_{PET\cdot NP}$, were adjusted for age, sex, and years of education and performed FDR correction at q as 0.05 (Benjamini & Hochberg, 1995). Additionally, Bonferroni correction was performed in the WD map (Bonferroni corrected adjusted $p < .01$) to confirm statistical robustness (Bonferroni, 1936).

2.8.3 | Measurement of centroid of cognition-related PET uptakes

We constructed a linear plot between the averaged PET-SUVR in each paired-voxels, which is defined as a link in each correlation matrix $D_{PET\cdot NP}$, and each NP across all CN at baseline to examine a linear trend between two variables at group level (Figure 1b). Then, we calculated a centroid of the averaged PET-SUVRs from the plot between the averaged PET-SUVRs in each paired-voxels and each NP score by considering the distribution of the plot in group level. The centroid was calculated by assessing cluster centroid locations in the plot distribution between the averaged PET-SUVRs and NP scores via k-means clustering analysis within MATLAB toolbox. The centroid value in each link was only calculated if the averaged PET-SUVRs in this link had significantly correlated with NP score in the correlation matrix $D_{PET\cdot NP}$ (Figure 1a,b). This centroid calculation was iterated for the number of all links of the correlation matrix $D_{PET\cdot NP}$. We obtained 6,848-by-6,848 centroid matrix $D_{Centroid}$ in each NP score in each type of PET correlation.

In order to visualize the effects of the graph theory-based measurements, the centroid values, in cognitive variability in CN, we calculated the sum of the centroid values in each voxel b by adding the centroid values across all links connected to the voxel b in the centroid matrix $D_{Centroid}$, excluding self-connection (Figure 1c). The sum of the centroid in all 6,848 voxels were calculated in each centroid matrix $D_{Centroid}$, then resampled to the corresponding GM voxels in the MNI template. Finally, we obtained the volume-based map of the sum of the centroid values derived from each centroid matrix $D_{Centroid}$ in group level. We resampled each volume-based map of the sum of the centroid values onto the group averaged cortical surface by mapping a value of middle point between inner and outer surfaces in each vertex point via FreeSurfer recon-all procedure (FreeSurfer version 6.0.0; http://surfer.nmr.mgh.harvard.edu/) (Figure 1c).

2.9 | Longitudinal analysis

We performed a similarity approach based on the centroid map to examine whether the PET uptakes were reliably associated with the cognitive impairment in CN at both baseline and 2-year FU. We performed spatial correlations between the centroid map and the individual averaged PET-SUVR images to determine the topological similarity between them, across all CN at both baseline and 2-year FU. Then, we used these spatial similarity scores from all individuals to investigate whether significant associations exist between PET patterns and cognitive scores in CN at baseline, and in an independent longitudinal sample.

2.9.1 | Measurement of similarity score

We measured the spatial similarity between the centroid map, which was defined by CN at baseline only, and a local corresponding voxel-based averaged PET-SUVR map of each individual across all CN at baseline and 2-year FU by using Pearson correlation analysis. First, we constructed a local voxel-based averaged PET-SUVR map by averaging a local voxel's PET-SUVR and the same voxel's PET-SUVR across all voxels in each individual in CN at baseline and 2-year FU. For example, if the centroid map is based on different PET modalities, each local voxel-based averaged PET-SUVR was calculated by averaging between a local PET-SUVR and the corresponding voxel's another PET-SUVR in each voxel in each individual level. If the centroid map is based on the single PET modality, we just used a single PET-SUVR map of each individual instead of the calculation of the local voxel-based averaged PET-SUVRs. Because each voxel's value of the centroid map was calculated by summing the centroid values across all possible associations between the one voxel and the rest of the GM voxels from the centroid matrix, the centroid map was based on the local-to-distributed voxel's PET correlations. Therefore, we used the local voxel-based averaged PET-SUVR maps, which were based on the local-to-local PET-SUVRs, to avoid circular dependency in the final analysis. Consequently, we obtained a similarity score for each individual across all CN at baseline and 2-year FU.

2.9.2 | Linear association between the similarity scores and cognitive scores

To better visualize whether the high similarity scores are significantly associated with the worsening of the cognitive test performances across individuals, we performed linear regression analysis between the similarity scores and cognitive test scores. All linear regression analyses were performed with SurfStat MATLAB toolbox (http://www.math.mcgill.ca/keith/surfstat). The group difference in slopes of the linear regression lines between the FU-matched CN at baseline and CN at 2-year FU data were tested by analysis of variance (ANOVA) within MATLAB toolbox.

3 | RESULTS

3.1 | Group demographics and clinical characteristics

All demographic characteristics and NP tests scores are described in Table 1. We found that most of our sample of CN displayed low levels of amyloid and tau at baseline (threshold of global FBP-SUVR ≥ 1.10 and mean tau-SUVR in composite ROIs > 1.25). There was no significant group difference in NP scores between 2-year FU data and FU-matched baseline data.

3.2 | Group averaged FBP-SUVR and tau-SUVR

A high group averaged FBP-SUVR was observed in CN at baseline, mainly in medial frontal cortex, PCC/precuneus, inferior temporal cortex, and lateral occipital cortex (Figure 2a). Compared to baseline, relatively higher group averaged FBP-SUVR was observed in temporal cortex, and part of parietal cortex in CN at 2-year FU (Figure 2b). A slightly higher group averaged tau-SUVR was observed mainly in wide areas of the temporal cortex, MTL, medial prefrontal cortex, and PCC in CN at baseline (Figure 2c). The group averaged tau-SUVR was more increased in CN at 2-year FU, partly in temporal cortex (Figure 2d).

We observed significant longitudinal changes between CN at 2-year FU and FU-matched baseline in tau-SUVR, but not obviously noted in FBP-SUVR (Supplementary Figure 3). We observed a significantly increased FBP-SUVR in only a few spots of cortical areas (Supplementary Figure 3a), while, a significantly increased tau-SUVR was noted in wide areas of the temporal cortex, prefrontal cortex, parietal cortex, and PCC in CN at 2-year FU compared with the FU-matched baseline (Supplementary Figure 3b).

3.3 | Graph theory-based PET correlation within single PET modality and between different PET modalities

We observed significant PET correlation within single PET modality, such as Aβ-to-Aβ and Tau-to-Tau correlations, as well as the PET correlation between different PET modalities, such as Aβ-to-Tau and Tau-to-Aβ correlation, in CN at baseline (FDR corrected $q < 0.05$, Figure 3). Spatial distributions of WD of the PET correlation within single PET modality, which was calculated by summation of all correlation coefficients in all possible links between each voxel and the rest of voxels, were observed across almost all cortical areas, excluding motor cortex, in CN at baseline (Figure 3a,b). A voxel with the high WD indicates that this voxel have the large number of connections to the rest of voxels, that means the PET-SUVR of this voxel is strongly correlated with the PET-SUVR of the rest of the paired voxels, broadly. A high WD of the PET correlation was noted mainly in both

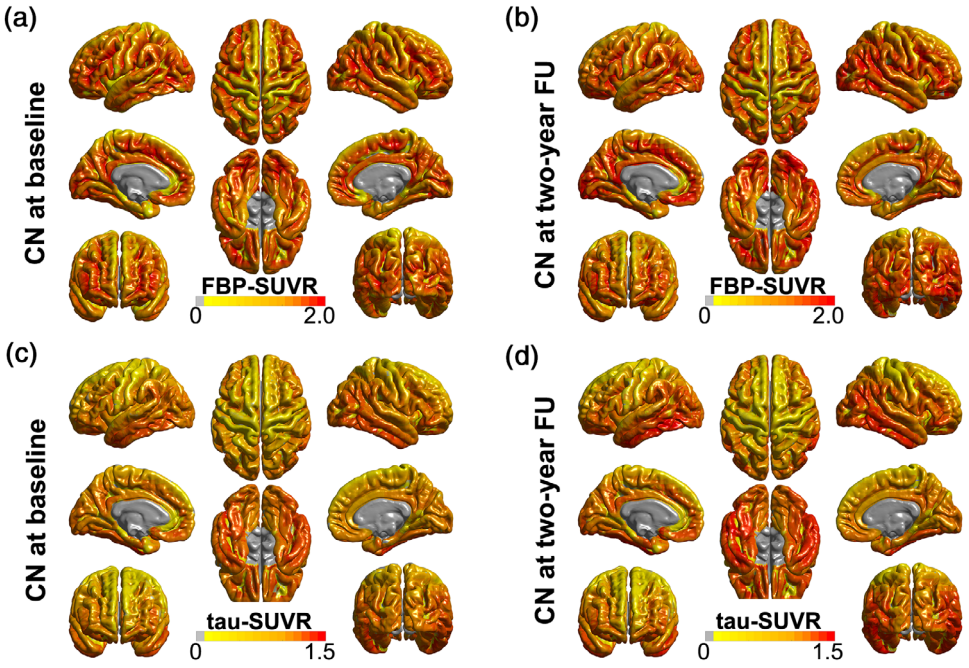

FIGURE 2 Surface-mapped group averaged (a) FBP-SUVR and (b) tau-SUVR in CN at all baseline and group averaged (c) FBP-SUVR and (d) tau-SUVR in CN at 2-year FU after performing PVC. Red color indicates high positron emission tomography (PET)-SUVR. CN, cognitively normal older adults; FBP, 18F-Florbetapir; FU, follow-up; PVC, partial volume correction; SUVR, standardized uptake value ratio; tau, F18-AV-1451

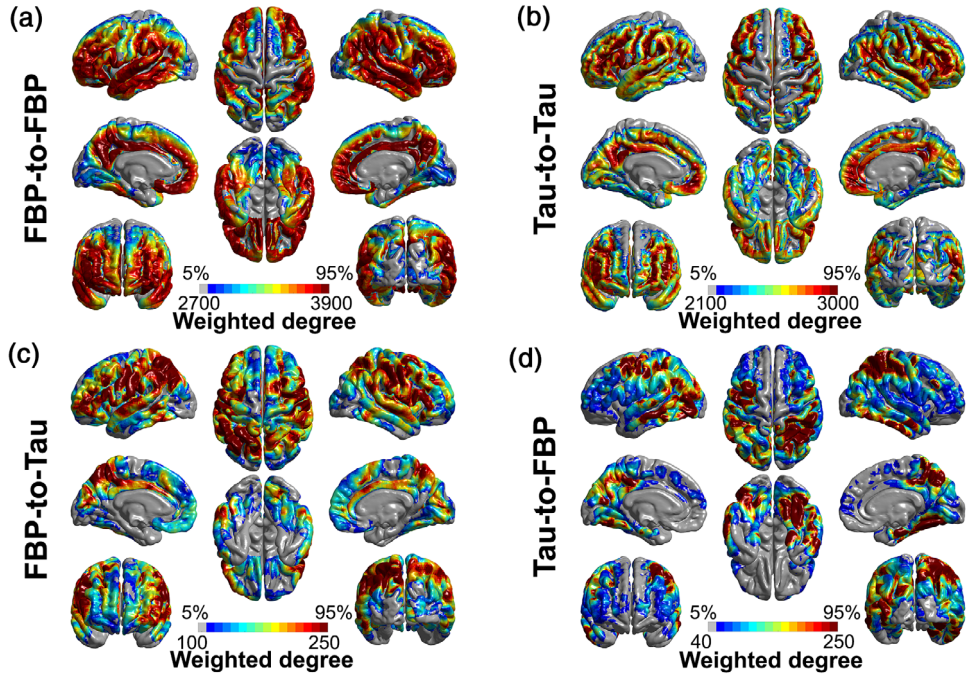

FIGURE 3 Weighted degree maps of positron emission tomography (PET) correlations in CN at baseline. Cortical distributions of FBP-to-FBP (a), Tau-to-Tau (b), FBP-to-Tau (c), and Tau-to-FBP (d) weighted degree maps in CN at baseline while adjusting for age, sex, and FBP-SUVR or tau-SUVR when appropriate in all paired-voxels. Only multiple comparison corrected significant correlation coefficients were included in the weighted degree maps (FDR corrected $q < 0.05$). Color bar indicates the weighted degree value; a high score indicates that the PET-SUVR of this surfaced-mapped local voxel is strongly correlated with the rest of voxels, broadly. CN, cognitively normal older adults; FBP, 18F-Florbetapir; FDR, False discovery rate; SUVR, standardized uptake value ratio; tau, F18-AV-1451

PCC/precuneus, medial frontal cortex, parietal cortex, and broad areas of temporal cortex in Aβ-to-Aβ correlation in CN at baseline (Figure 3a). Compared to Aβ-to-Aβ correlation, Tau-to-Tau correlation showed relatively low WD in the temporal cortex, precuneus, and frontal cortex in CN at baseline (Figure 3b).

A spatial distribution of WD of the PET correlations between different PET modalities, such as Aβ-to-Tau and Tau-to-Aβ correlations, was shown in large areas of cortical regions in CN at baseline, but that showed relatively lower PET correlations compared with the PET correlations within single PET modality (Figure 3c,d). High WD was observed mainly in the left lateral parietal cortex, left precuneus, left orbitofrontal cortex, and both superior temporal cortices in Aβ-to-Tau correlation in CN at baseline (Figure 3c). A spatial distribution of WD of Tau-to-Aβ correlation was less spread out than the other PET correlations, but showed more intensive WD pattern in both inferior temporal cortices, both precuneus, right fusiform gyrus, and right lateral parietal cortex in CN at baseline (Figure 3d).

3.4 | Relationship between the information of the graph theory-based correlation matrix and cognitive variability

There was a significant positive PET-to-NP correlation between averaged PET-SUVRs, the mean values between FBP-SUVR of a local voxel and tau-SUVR of the rest of voxels, and ADAS-Cog scores in the type of Aβ-to-Tau correlation after controlling for years of education in CN at baseline (FDR corrected $q < 0.05$). In contrast, no significant correlation between the averaged PET-SUVRs and any NP scores was found in other types of PET correlations, such as Aβ-to-Aβ, Tau-to-Tau, and Tau-to-Aβ correlations, after performing FDR correction in CN at baseline. In this analysis, a voxel with high WD of the PET-to-NP correlation indicates that the averaged PET-SUVR from the different PET modalities between this voxel and the rest of the voxels is strongly correlated with the NP scores, broadly. Thus, high WD reflects the strong effects of the averaged PET-SUVR between different PET modalities between different voxels in cognitive scores. We found that the high averaged PET-SUVRs derived from Aβ-to-Tau connectivity was significantly correlated with high ADAS-Cog scores in left superior temporal cortex, left inferior cortex, left superior parietal cortex, part of left PCC/precuneus, part of right superior temporal cortex, right middle parietal cortex, right precuneus, both middle frontal cortices, and both cuneus (Figure 4a). Similar topology remains significant after performing post hoc Bonferroni correction (Figure 4b).

3.5 | Measurement of cognition-related PET uptakes at baseline and longitudinal FU

Of note, in this section, an individual with high similarity score indicates that the uptake spatial pattern of the averaged Aβ and tau PET-SUVRs is well overlapped to the centroid map, which reflects the

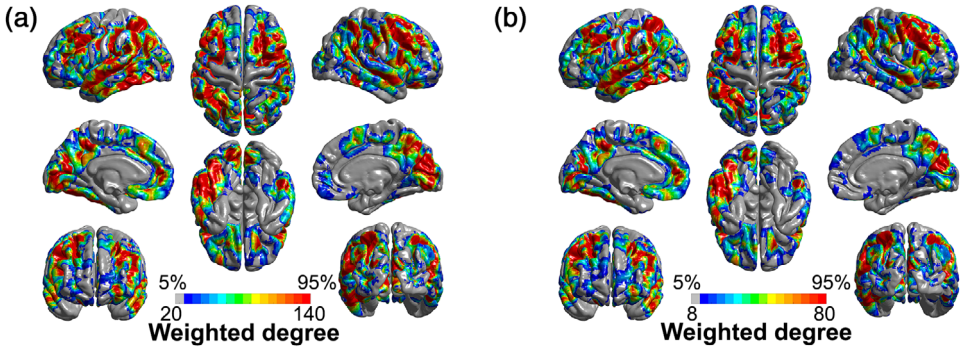

FIGURE 4 Weighted degree maps of positron emission tomography (PET)-to-NP correlations between the averaged PET-SUVRs and ADAS-Cog scores in CN at baseline adjusted by age, sex, and years of education. (a) Only multiple comparison corrected significant correlation coefficients were included in the weighted degree map (FDR corrected $q < 0.05$). (b) Bonferroni correction was also performed in the weighted degree map (Bonferroni corrected adjusted $p < .01$) to confirm statistical robustness. Color bar indicates the weighted degree of PET-to-NP correlations; a high score indicates that the averaged PET-SUVRs between this voxel and the rest of the voxels are strongly correlated with the ADAS-Cog scores. ADAS-Cog, Alzheimer's Disease Assessment Scale-Cognitive Subscale; CN, cognitively normal older adults; FBP, 18F-Florbetapir; FDR, False discovery rate; NP, neuropsychological scores; SUVR, standardized uptake value ratio; tau, F18-AV-1451

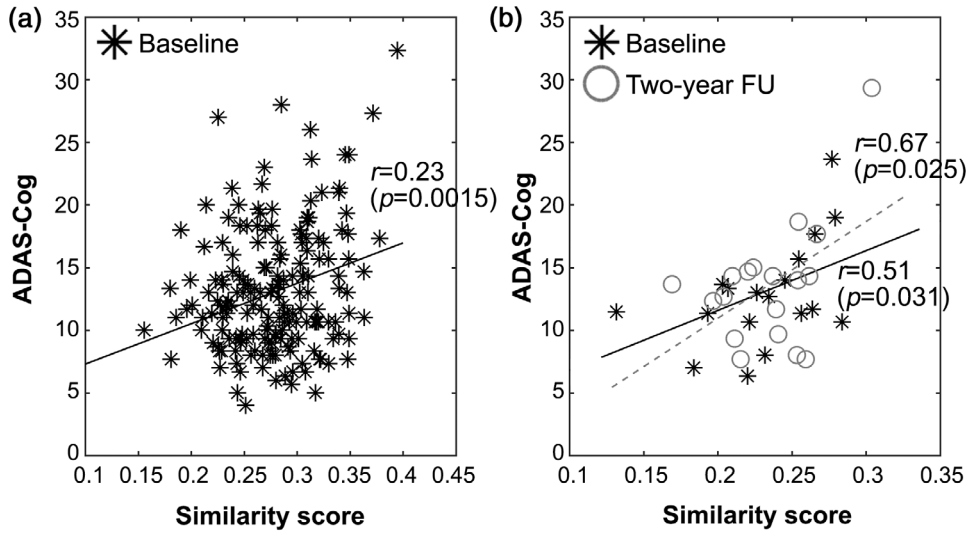

FIGURE 5 Linear regression associations between similarity scores and ADAS-Cog in CN at baseline and 2-year FU time point. (a) A significant positive association between the similarity score and ADAS-Cog was noted in CN at baseline ($t_{(182)} = 3.22$, $p = .0015$). (b) Similar positive association was noted in both 2-year FU ($t_{(16)} = 2.41$, $p = .025$), as well as FU-matched baseline ($t_{(16)} = 2.36$, $p = .031$). ADAS-Cog, Alzheimer's Disease Assessment Scale-Cognitive Subscale; CN, cognitively normal older adults; FBP, 18F-Florbetapir; FU, follow-up; SUVR, standardized uptake value ratio; tau, F18-AV-1451

information of the spatial patterns of cognitive impairment-related PET uptakes. Thus, the high similarity score reflects the worsening of the cognitive test performance. We found that increased spatial similarity scores were significantly associated with increased ADAS-Cog score in CN at baseline ($t_{(182)} = 3.22$, $p = .0015$, Figure 5a). A similar linear association between the similarity score and ADAS-Cog was observed in CN at 2-year FU ($t_{(16)} = 2.41$, $p = .025$, Figure 5b) as well as in FU-matched baseline ($t_{(16)} = 2.36$, $p = .031$, Figure 5b). There is no significant slope difference between FU-matched baseline and 2-year FU groups after performing ANOVA. Although there was no significant slope difference between FU-matched baseline and 2-year FU, the slope was slightly higher in 2-year FU compared with the FU-matched baseline (Figure 5b).

4 | DISCUSSION

AD is a neurodegenerative disorder in which the network-level accumulation of Aβ and tau pathology seems to play a critical role in the appearance of cognitive symptoms. Currently, we believe that close and interdigitated spatial interactions of Aβ and tau within neural circuits might be a better indicator of early preclinical processes and

cognitive decline of aging populations. Following this line of research, in the present study, we used a novel graph-theory approach to investigate brain network profiles of Aβ and tau PET imaging and cognitive scores. We found striking positive correlations between the Aβ-to-Tau interactions and ADAS-Cog score, which is the most widely used measure to assess multiple cognitive domains in AD (Mohs et al., 1997a, 1997b; Rosen, Mohs, & Davis, 1984) and was developed to measure general cognition, including verbal memory, nonverbal memory, planning an executive function, attention and concentration, praxis, and orientation (Mohs et al., 1997a, 1997b; Podhorna, Krahnke, Shear, Harrison, & Alzheimer's Disease Neuroimaging, 2016; Skinner et al., 2012). Particularly, we observed a high correlation between Aβ-to-Tau interactions and ADAS-Cog in the temporal cortex. This is consistent with the previous findings that show not only a significant association between tau and cognitive impairment in MTL (Sepulcre et al., 2018), but also that these cognition-related tau accumulation in MTL are associated with an increased Aβ burden in older adults (Schöll et al., 2016; Sperling et al., 2019) or mild-to-moderate AD (Johnson et al., 2016). Other areas in the fronto-parieto-occipital cortices displayed similar network-based ADAS-Cog associations. Previous literature has shown a strong relationship between local Aβ and local tau in probable AD (Iaccarino et al., 2018), and a strong association between the inferior temporal tau accumulation and distributed Aβ accumulation in older adults (Sepulcre et al., 2016; Sperling et al., 2019). Thus, although a significant association between both pathology accumulations and cognitive decline was reported mainly in MTL in previous studies (Johnson et al., 2016; Schöll et al., 2016; Sperling et al., 2019), the cognition-related tau accumulation (Ossenkoppele et al., 2019; Sepulcre et al., 2018) or Aβ accumulation (Schöll et al., 2016) in regions beyond MTL, such as the parietal cortex, frontal cortex, or occipital cortex, was also reported in several studies. These selective associations of cognitive impairment or neurodegenerative changes with AD pathology accumulations depend on the AD severity (Ossenkoppele et al., 2019) and Braak stages (Schöll et al., 2016). Thus, we believe that high associations of Aβ-to-Tau interactions and ADAS-Cog scores in MTL-related regions, as well as the fronto-parieto-occipital lobes, may indicate specific states of network interactions, from local Aβ toward distributed tau, that potentiates neurodegenerative and cognitive changes via Aβ-triggered tau (Duyckaerts, 2011; Ittner & Götz, 2011; Jacobs et al., 2018; Small & Duff, 2008).

Our findings show that the cross-talking of Aβ-to-Tau better explains the initial cognitive changes of CN compared to brain network profiles derived from single PET modalities, such as Aβ-to-Aβ, or Tau-to-Tau. The effects of Aβ pathology in cognitive decline generally appeared in prodromal AD and dementia, rather than in cognitively healthy older adults (Ossenkoppele et al., 2019). Therefore, the absence of the significant PET-to-NP correlation in type of Aβ-to-Aβ may be caused by the insufficient Aβ accumulation in CN at baseline, which seems to be a late phenomenon. Similarly, no significant PET-to-NP correlation in type of tau-to-tau was observed in CN at baseline. Sperling et al. (2019) showed the association between cognitive decline and tau accumulation in MTL in older adults; however, an increased tau accumulation in the temporal cortex was commonly observed in Braak stage of III or IV (Braak, Alafuzoff, Arzberger, Kretzschmar, & Del Tredici, 2006; Braak & Braak, 1991b, 1995) and in tau PET image (Johnson et al., 2016). Thus, a relatively weaker tau-to-tau correlation in MTL may also explain the absence of the significant PET-to-NP correlation in our study. Finally, we did not observe significant PET-to-NP correlations in the type of Tau-to-Aβ. As we controlled tau-SUVR effects in FBP-SUVRs of all possible paired-voxels when we measured the correlation between the averaged PET-SUVR and ADAS-Cog scores in types of Tau-to-Aβ correlation, one possible explanation is that tau-independent Aβ may not sufficiently contribute to the initial cognitive changes in CN at baseline even though tau-controlled FBP-SUVR showed a strong association with the local tau-SUVR in MTL.

Currently, the major concern to investigate the relationship between Aβ and tau accumulations is the spatial inconsistencies between the two brain pathologies. The lack of spatial correlation or overlap between a local Aβ and the corresponding local tau accumulations has been reported in imaging studies, which makes it difficult to investigate their potential synergistic effects on cognitive decline in aging. The benefit of conducting a graph theory-based approach is that it provides a high-resolution strategy to relate these two unmatched anatomies. Our proposed graph theory-based approach measures the local-to-distributed correlations within and between Aβ and tau PET modalities, thus solving the spatial inconsistency between them. In this network-based study, we only observed significant findings with ADAS-Cog scores. The absence of significance in the correlation analysis between the averaged PET-SUVRs and other NP scores included in the study is somewhat surprising. It is possible that ADAS-Cog is the most sensitive to test in this work due to its multi-domain nature. However, future studies are needed to examine other PET-to-NP correlations by assessing multiple cognitive measurements in both cognitively normal and impaired older adults through multiple longitudinal FUs. Moreover, we used multicenter ADNI data, which may have a potential bias in PET images caused by multiple scanner types or visit sites. We observed consistency in the cortical distribution of the mean tau-SUVRs and mean FBP-SUVRs across three scanner types in CN at baseline (Supplementary Figure 1). We performed one-way ANOVA to determine whether there are any statistically significant differences in the means of PET-SUVRs of GM between the three types of scanner, and we found no significant difference in mean tau-SUVR or mean FBP-SUVR between three types of scanners (Supplementary Figure 2). No meaningful trends of group difference between two groups in the mean PET-SUVRs was noted (Supplementary Figure 2). Nevertheless, future studies should apply similar network PET-based strategies within unicenter data to avoid potential scanner biases. Our study has an additional limitation: we mainly focused on a large CN sample at baseline, and a relatively small longitudinal sample from ADNI-3 study dataset. Therefore, larger number of FU individuals should be used and tested in future studies.

5 | CONCLUSION

We examined network interaction patterns within single PET modality, such as Aβ-to-Aβ or Tau-to-Tau correlations, and between different PET modalities, such as Aβ-to-Tau or Tau-to-Aβ, at high-resolution (voxel-level) in CN, using a graph theory-based analysis. We observed that the PET uptakes derived from Aβ-to-Tau interdigitations were significantly associated with ADAS-Cog in AD vulnerable brain areas, a finding confirmed by our longitudinal investigation. Therefore, our work suggests the preceding contribution of network interactions between Aβ and tau deposits to explain initial cognitive changes in CN prior to the conversion of dementia.

ACKNOWLEDGMENT

This research was supported by grants from the National Institutes of Health (NIH) (R01AG061811, and R01AG061445 to J. S.).

CONFLICT OF INTEREST

The authors declare no potential conflict of interest.

AUTHOR CONTRIBUTIONS

Chan-Mi Kim: Study concept and design, analysis of the data, interpretation of the data, drafting of manuscript, revision of the manuscript. **Victor Montal**: Data quality check and analysis of the data. **Ibai Diez**: Analysis of the data. **William Orwig**: Assistant of the revision of the manuscript. **Jorge Sepulcre**: Study concept and design and revision of the manuscript.

DATA AVAILABILITY STATEMENT

Data used in preparation of this article were obtained from the Alzheimer's Disease Neuroimaging Initiative (ADNI) database (adni.loni.usc.edu). As such, the investigators within the ADNI contributed to the design and implementation of ADNI and/or provided data but did not participate in analysis or writing of this report. A complete listing of ADNI investigators can be found at: http://adni.loni.usc.edu/wp-content/uploads/how_to_apply/ADNI_Acknowledgement_List.pdf.

ORCID

Chan-Mi Kim https://orcid.org/0000-0001-5686-1668

REFERENCES

Arnold, S. E., Hyman, B. T., Flory, J., Damasio, A. R., & van Hoesen, G. W. (1991). The topographical and neuroanatomical distribution of neurofibrillary tangles and neuritic plaques in the cerebral cortex of patients with Alzheimer's disease. *Cerebral Cortex*, *1*(1), 103–116.

Ballard, C., Gauthier, S., Corbett, A., Brayne, C., Aarsland, D., & Jones, E. (2011). Alzheimer's disease. *Lancet (London, England)*, *377*(9770), 1019–1031.

Barthel, H., Gertz, H.-J., Dresel, S., Peters, O., Bartenstein, P., Buerger, K., … Reininger, C. (2011). Cerebral amyloid-β PET with florbetaben (18F) in patients with Alzheimer's disease and healthy controls: A multicentre phase 2 diagnostic study. *The Lancet Neurology*, *10*(5), 424–435.

Benjamini, Y., & Hochberg, Y. (1995). Controlling the false discovery rate: A practical and powerful approach to multiple testing. *Journal of the Royal Statistical Society. Series B (Methodological)*, *57*, 289–300.

Bennett, R. E., DeVos, S. L., Dujardin, S., Corjuc, B., Gor, R., Gonzalez, J., … Carlson, G. A. (2017). Enhanced tau aggregation in the presence of amyloid β. *The American Journal of Pathology*, *187*(7), 1601–1612.

Bonferroni, C. (1936). Teoria statistica delle classi e calcolo delle probabilita. In *Pubblicazioni del R Istituto Superiore di Scienze Economiche e Commericiali di Firenze* (Vol. 8, pp. 3–62).

Braak, H., Alafuzoff, I., Arzberger, T., Kretzschmar, H., & del Tredici, K. (2006). Staging of Alzheimer disease-associated neurofibrillary pathology using paraffin sections and immunocytochemistry. *Acta Neuropathologica*, *112*(4), 389–404.

Braak, H., & Braak, E. (1991a). Demonstration of amyloid deposits and neurofibrillary changes in whole brain sections. *Brain Pathology*, *1*(3), 213–216.

Braak, H., & Braak, E. (1991b). Neuropathological stageing of Alzheimer-related changes. *Acta Neuropathologica*, *82*(4), 239–259.

Braak, H., & Braak, E. (1995). Staging of Alzheimer's disease-related neurofibrillary changes. *Neurobiology of Aging*, *16*(3), 271–278.

Braak, H., & del Tredici, K. (2011). Alzheimer's pathogenesis: Is there neuron-to-neuron propagation? *Acta Neuropathologica*, *121*(5), 589–595.

Brier, M. R., Gordon, B., Friedrichsen, K., McCarthy, J., Stern, A., Christensen, J., … Hassenstab, J. (2016). Tau and Aβ imaging, CSF measures, and cognition in Alzheimer's disease. *Science Translational Medicine*, *8*(338), 338ra366–338ra366.

Chien, D. T., Bahri, S., Szardenings, A. K., Walsh, J. C., Mu, F., Su, M.-Y., … Kolb, H. C. (2013). Early clinical PET imaging results with the novel PHF-tau radioligand [F-18]-T807. *Journal of Alzheimer's Disease*, *34*(2), 457–468.

Clark, C. M., Pontecorvo, M. J., Beach, T. G., Bedell, B. J., Coleman, R. E., Doraiswamy, P. M., … Sadowsky, C. H. (2012). Cerebral PET with florbetapir compared with neuropathology at autopsy for detection of neuritic amyloid-β plaques: A prospective cohort study. *The Lancet Neurology*, *11*(8), 669–678.

Clark, C. M., Schneider, J. A., Bedell, B. J., Beach, T. G., Bilker, W. B., Mintun, M. A., … Flitter, M. L. (2011). Use of florbetapir-PET for imaging β-amyloid pathology. *JAMA*, *305*(3), 275–283.

Clavaguera, F., Bolmont, T., Crowther, R. A., Abramowski, D., Frank, S., Probst, A., … Staufenbiel, M. (2009). Transmission and spreading of tauopathy in transgenic mouse brain. *Nature Cell Biology*, *11*(7), 909–913.

Crane, P. K., Carle, A., Gibbons, L. E., Insel, P., Mackin, R. S., Gross, A., … Alzheimer's Disease Neuroimaging Initiative. (2012). Development and assessment of a composite score for memory in the Alzheimer's Disease Neuroimaging Initiative (ADNI). *Brain Imaging and Behavior*, *6*(4), 502–516. https://doi.org/10.1007/s11682-012-9186-z

Dale, A. M., Fischl, B., & Sereno, M. I. (1999). Cortical surface-based analysis. I. Segmentation and surface reconstruction. *NeuroImage*, *9*(2), 179–194. https://doi.org/10.1006/nimg.1998.0395

de Calignon, A., Polydoro, M., Suárez-Calvet, M., William, C., Adamowicz, D. H., Kopeikina, K. J., … Carlson, G. A. (2012). Propagation of tau pathology in a model of early Alzheimer's disease. *Neuron*, *73*(4), 685–697.

Desikan, R. S., Segonne, F., Fischl, B., Quinn, B. T., Dickerson, B. C., Blacker, D., … Killiany, R. J. (2006). An automated labeling system for subdividing the human cerebral cortex on MRI scans into gyral based regions of interest. *NeuroImage*, *31*(3), 968–980. https://doi.org/10.1016/j.neuroimage.2006.01.021

Duyckaerts, C. (2011). Tau pathology in children and young adults: Can you still be unconditionally Baptist?. *Acta Neuropathologica*. *121*(2), 145–147.

Fagan, A. M., Roe, C. M., Xiong, C., Mintun, M. A., Morris, J. C., & Holtzman, D. M. (2007). Cerebrospinal fluid tau/β-amyloid42 ratio as a

prediction of cognitive decline in nondemented older adults. *Archives of Neurology*, *64*(3), 343–349.

Fischl, B., Liu, A., & Dale, A. M. (2001). Automated manifold surgery: Constructing geometrically accurate and topologically correct models of the human cerebral cortex. *IEEE Transactions on Medical Imaging*, *20*(1), 70–80. https://doi.org/10.1109/42.906426

Fischl, B., Salat, D. H., Busa, E., Albert, M., Dieterich, M., Haselgrove, C., … Dale, A. M. (2002). Whole brain segmentation: Automated labeling of neuroanatomical structures in the human brain. *Neuron*, *33*(3), 341–355.

Fischl, B., Salat, D. H., van der Kouwe, A. J., Makris, N., Ségonne, F., Quinn, B. T., & Dale, A. M. (2004). Sequence-independent segmentation of magnetic resonance images. *NeuroImage*, *23*, S69–S84.

Fischl, B., Sereno, M. I., Tootell, R. B., & Dale, A. M. (1999). High-resolution intersubject averaging and a coordinate system for the cortical surface. *Human Brain Mapping*, *8*(4), 272–284.

Fischl, B., van der Kouwe, A., Destrieux, C., Halgren, E., Segonne, F., Salat, D. H., … Dale, A. M. (2004). Automatically parcellating the human cerebral cortex. *Cerebral Cortex*, *14*(1), 11–22.

Fleisher, A. S., Chen, K., Quiroz, Y. T., Jakimovich, L. J., Gomez, M. G., Langois, C. M., … Lee, W. (2015). Associations between biomarkers and age in the presenilin 1 E280A autosomal dominant Alzheimer disease kindred: A cross-sectional study. *JAMA Neurology*, *72*(3), 316–324.

Folstein, M. F., Folstein, S. E., & McHugh, P. R. (1975). "Mini-mental state". A practical method for grading the cognitive state of patients for the clinician. *Journal of Psychiatric Research*, *12*(3), 189–198. https://doi.org/10.1016/0022-3956(75)90026-6

Ghoshal, N., García-Sierra, F., Wuu, J., Leurgans, S., Bennett, D. A., Berry, R. W., & Binder, L. I. (2002). Tau conformational changes correspond to impairments of episodic memory in mild cognitive impairment and Alzheimer's disease. *Experimental Neurology*, *177*(2), 475–493.

Gibbons, L. E., Carle, A. C., Mackin, R. S., Harvey, D., Mukherjee, S., Insel, P., … Alzheimer's Disease Neuroimaging Initiative. (2012). A composite score for executive functioning, validated in Alzheimer's Disease Neuroimaging Initiative (ADNI) participants with baseline mild cognitive impairment. *Brain Imaging and Behavior*, *6*(4), 517–527. https://doi.org/10.1007/s11682-012-9176-1

Götz, J., Chen, F. V., van Dorpe, J., & Nitsch, R. (2001). Formation of neurofibrillary tangles in P301L tau transgenic mice induced by Aβ42 fibrils. *Science*, *293*(5534), 1491–1495.

Greve, D. N., Salat, D. H., Bowen, S. L., Izquierdo-Garcia, D., Schultz, A. P., Catana, C., … Johnson, K. A. (2016). Different partial volume correction methods lead to different conclusions: An (18)F-FDG-PET study of aging. *NeuroImage*, *132*, 334–343. https://doi.org/10.1016/j.neuroimage.2016.02.042

Guo, J. L., & Lee, V. M. (2014). Cell-to-cell transmission of pathogenic proteins in neurodegenerative diseases. *Nature Medicine*, *20*(2), 130–138. https://doi.org/10.1038/nm.3457

Hanseeuw, B. J., Betensky, R. A., Jacobs, H. I., Schultz, A. P., Sepulcre, J., Becker, J. A., … Mormino, E. C. (2019). Association of amyloid and tau with cognition in preclinical Alzheimer disease: A longitudinal study. *JAMA Neurology*, *76*(8), 915–924.

He, Z., Guo, J. L., McBride, J. D., Narasimhan, S., Kim, H., Changolkar, L., … Dengler, C. (2018). Amyloid-β plaques enhance Alzheimer's brain tau-seeded pathologies by facilitating neuritic plaque tau aggregation. *Nature Medicine*, *24*(1), 29–38.

Hurtado, D. E., Molina-Porcel, L., Iba, M., Aboagye, A. K., Paul, S. M., Trojanowski, J. Q., & Lee, V. M.-Y. (2010). Aβ accelerates the spatiotemporal progression of tau pathology and augments tau amyloidosis in an Alzheimer mouse model. *The American Journal of Pathology*, *177*(4), 1977–1988.

Iaccarino, L., Tammewar, G., Ayakta, N., Baker, S. L., Bejanin, A., Boxer, A. L., … Lazaris, A. (2018). Local and distant relationships between amyloid, tau and neurodegeneration in Alzheimer's Disease. *NeuroImage: Clinical*, *17*, 452–464.

Iba, M., Guo, J. L., McBride, J. D., Zhang, B., Trojanowski, J. Q., & Lee, V. M.-Y. (2013). Synthetic tau fibrils mediate transmission of neurofibrillary tangles in a transgenic mouse model of Alzheimer's-like tauopathy. *Journal of Neuroscience*, *33*(3), 1024–1037.

Iqbal, K., & Grundke-Iqbal, I. (2002). Neurofibrillary pathology leads to synaptic loss and not the other way around in Alzheimer disease. *Journal of Alzheimer's Disease*, *4*(3), 235–238.

Ittner, L. M., & Götz, J. (2011). Amyloid-β and tau—A toxic pas de deux in Alzheimer's disease. *Nature Reviews Neuroscience*, *12*(2), 67–72.

Jack, C. R., Jr., Knopman, D. S., Jagust, W. J., Shaw, L. M., Aisen, P. S., Weiner, M. W., … Trojanowski, J. Q. (2010). Hypothetical model of dynamic biomarkers of the Alzheimer's pathological cascade. *The Lancet Neurology*, *9*(1), 119–128.

Jacobs, H. I., Hedden, T., Schultz, A. P., Sepulcre, J., Perea, R. D., Amariglio, R. E., … Johnson, K. A. (2018). Structural tract alterations predict downstream tau accumulation in amyloid-positive older individuals. *Nature Neuroscience*, *21*(3), 424–431.

Jansen, W. J., Ossenkoppele, R., Knol, D. L., Tijms, B. M., Scheltens, P., Verhey, F. R., … Alcolea, D. (2015). Prevalence of cerebral amyloid pathology in persons without dementia: A meta-analysis. *JAMA*, *313*(19), 1924–1938.

Johnson, K. A., Minoshima, S., Bohnen, N. I., Donohoe, K. J., Foster, N. L., Herscovitch, P., … Pappas, V. (2013). Update on appropriate use criteria for amyloid PET imaging: Dementia experts, mild cognitive impairment, and education. *Journal of Nuclear Medicine*, *54*(7), 1011–1013.

Johnson, K. A., Schultz, A., Betensky, R. A., Becker, J. A., Sepulcre, J., Rentz, D., … Papp, K. (2016). Tau positron emission tomographic imaging in aging and early Alzheimer's disease. *Annals of Neurology*, *79*(1), 110–119.

Joshi, A. D., Pontecorvo, M. J., Clark, C. M., Carpenter, A. P., Jennings, D. L., Sadowsky, C. H., … Arora, A. (2012). Performance characteristics of amyloid PET with florbetapir F 18 in patients with Alzheimer's disease and cognitively normal subjects. *Journal of Nuclear Medicine*, *53*(3), 378–384.

Kim, H.-R., Lee, P., Seo, S. W., Roh, J. H., Oh, M., Oh, J. S., … Jeong, Y. (2019). Comparison of amyloid β and Tau spread models in Alzheimer's Disease. *Cerebral Cortex*, *29*(10), 4291–4302.

Klunk, W. E., Engler, H., Nordberg, A., Wang, Y., Blomqvist, G., Holt, D. P., … Estrada, S. (2004). Imaging brain amyloid in Alzheimer's disease with Pittsburgh compound-B. *Annals of Neurology*, *55*(3), 306–319.

Landau, S. M., Mintun, M. A., Joshi, A. D., Koeppe, R. A., Petersen, R. C., Aisen, P. S., … Alzheimer's Disease Neuroimaging Initiative. (2012). Amyloid deposition, hypometabolism, and longitudinal cognitive decline. *Annals of Neurology*, *72*(4), 578–586.

Lewis, J., Dickson, D. W., Lin, W.-L., Chisholm, L., Corral, A., Jones, G., … Yager, D. (2001). Enhanced neurofibrillary degeneration in transgenic mice expressing mutant tau and APP. *Science*, *293*(5534), 1487–1491.

Marquié, M., Normandin, M. D., Vanderburg, C. R., Costantino, I. M., Bien, E. A., Rycyna, L. G., … Debnath, M. L. (2015). Validating novel tau positron emission tomography tracer [F-18]-AV-1451 (T807) on postmortem brain tissue. *Annals of Neurology*, *78*(5), 787–800.

Meltzer, C. C., Zubieta, J. K., Links, J. M., Brakeman, P., Stumpf, M. J., & Frost, J. J. (1996). MR-based correction of brain PET measurements for heterogeneous gray matter radioactivity distribution. *Journal of Cerebral Blood Flow and Metabolism*, *16*(4), 650–658. https://doi.org/10.1097/00004647-199607000-00016

Mishra, S., Gordon, B. A., Su, Y., Christensen, J., Friedrichsen, K., Jackson, K., … Benzinger, T. L. S. (2017). AV-1451 PET imaging of tau pathology in preclinical Alzheimer disease: Defining a summary measure. *NeuroImage*, *161*, 171–178. https://doi.org/10.1016/j.neuroimage.2017.07.050

Mitchell, T. W., Mufson, E. J., Schneider, J. A., Cochran, E. J., Nissanov, J., Han, L. Y., … Bennett, D. A. (2002). Parahippocampal tau pathology in healthy aging, mild cognitive impairment, and early Alzheimer's disease. *Annals of Neurology*, *51*(2), 182–189.

Mohs, R. C., Knopman, D., Petersen, R. C., Ferris, S. H., Ernesto, C., Grundman, M., … Clark, C. (1997a). Development of cognitive instruments for use in clinical trials of antidementia drugs: Additions to the Alzheimer's Disease Assessment Scale that broaden its scope. *Alzheimer Disease and Associated Disorders*, *11*, 13–21.

Mohs, R. C., Knopman, D., Petersen, R. C., Ferris, S. H., Ernesto, C., Grundman, M., … Thal, L. J. (1997b). Development of cognitive instruments for use in clinical trials of antidementia drugs: Additions to the Alzheimer's Disease Assessment Scale that broaden its scope. The Alzheimer's Disease Cooperative Study. *Alzheimer Disease and Associated Disorders*, *11*(Suppl 2), S13–S21.

Muller-Gartner, H. W., Links, J. M., Prince, J. L., Bryan, R. N., McVeigh, E., Leal, J. P., … Frost, J. J. (1992). Measurement of radiotracer concentration in brain gray matter using positron emission tomography: MRI-based correction for partial volume effects. *Journal of Cerebral Blood Flow and Metabolism*, *12*(4), 571–583. https://doi.org/10.1038/jcbfm.1992.81

Nelson, P. T., Alafuzoff, I., Bigio, E. H., Bouras, C., Braak, H., Cairns, N. J., … Tredici, K. D. (2012). Correlation of Alzheimer disease neuropathologic changes with cognitive status: A review of the literature. *Journal of Neuropathology & Experimental Neurology*, *71*(5), 362–381.

Ossenkoppele, R., Smith, R., Ohlsson, T., Strandberg, O., Mattsson, N., Insel, P. S., … Hansson, O. (2019). Associations between tau, Aβ, and cortical thickness with cognition in Alzheimer disease. *Neurology*, *92*(6), e601–e612.

Pike, K. E., Savage, G., Villemagne, V. L., Ng, S., Moss, S. A., Maruff, P., … Rowe, C. C. (2007). β-Amyloid imaging and memory in non-demented individuals: Evidence for preclinical Alzheimer's disease. *Brain*, *130*(11), 2837–2844.

Podhorna, J., Krahnke, T., Shear, M., Harrison, J. E., & Alzheimer's Disease Neuroimaging Initiative. (2016). Alzheimer's Disease Assessment Scale-cognitive subscale variants in mild cognitive impairment and mild Alzheimer's disease: Change over time and the effect of enrichment strategies. *Alzheimer's Research & Therapy*, *8*, 8. https://doi.org/10.1186/s13195-016-0170-5

Pontecorvo, M. J., Devous, M. D., Sr., Navitsky, M., Lu, M., Salloway, S., Schaerf, F. W., … Lim, N. C. (2017). Relationships between flortaucipir PET tau binding and amyloid burden, clinical diagnosis, age and cognition. *Brain*, *140*(3), 748–763.

Quiroz, Y. T., Sperling, R. A., Norton, D. J., Baena, A., Arboleda-Velasquez, J. F., Cosio, D., … Miller, J. B. (2018). Association between amyloid and tau accumulation in young adults with autosomal dominant Alzheimer disease. *JAMA Neurology*, *75*(5), 548–556.

Resnick, S. M., Sojkova, J., Zhou, Y., An, Y., Ye, W., Holt, D. P., … Wong, D. F. (2010). Longitudinal cognitive decline is associated with fibrillar amyloid-beta measured by [11C]PiB. *Neurology*, *74*(10), 807–815. https://doi.org/10.1212/WNL.0b013e3181d3e3e9

Rey, A. (1958). *L'examen clinique en psychologie*. [The clinical examination in psychology]. Presses Universitaries De France.

Rolstad, S., Berg, A. I., Bjerke, M., Johansson, B., Zetterberg, H., & Wallin, A. (2013). Cerebrospinal fluid biomarkers mirror rate of cognitive decline. *Journal of Alzheimer's Disease*, *34*(4), 949–956.

Rosen, W. G., Mohs, R. C., & Davis, K. L. (1984). A new rating scale for Alzheimer's disease. *The American Journal of Psychiatry*, *141*(11), 1356–1364. https://doi.org/10.1176/ajp.141.11.1356

Rousset, O. G., Ma, Y., & Evans, A. C. (1998). Correction for partial volume effects in PET: Principle and validation. *Journal of Nuclear Medicine*, *39*(5), 904–911.

Schöll, M., Lockhart, S. N., Schonhaut, D. R., O'Neil, J. P., Janabi, M., Ossenkoppele, R., … Schwimmer, H. D. (2016). PET imaging of tau deposition in the aging human brain. *Neuron*, *89*(5), 971–982.

Ségonne, F., Dale, A. M., Busa, E., Glessner, M., Salat, D., Hahn, H. K., & Fischl, B. (2004). A hybrid approach to the skull stripping problem in MRI. *NeuroImage*, *22*(3), 1060–1075.

Selkoe, D. J. (2002). Alzheimer's disease is a synaptic failure. *Science*, *298*(5594), 789–791.

Sepulcre, J., Grothe, M. J., d'Oleire Uquillas, F., Ortiz-Teran, L., Diez, I., Yang, H. S., … Johnson, K. A. (2018). Neurogenetic contributions to amyloid beta and tau spreading in the human cortex. *Nature Medicine*, *24*(12), 1910–1918. https://doi.org/10.1038/s41591-018-0206-4

Sepulcre, J., Schultz, A. P., Sabuncu, M., Gomez-Isla, T., Chhatwal, J., Becker, A., … Johnson, K. A. (2016). In vivo tau, amyloid, and gray matter profiles in the aging brain. *Journal of Neuroscience*, *36*(28), 7364–7374.

Skinner, J., Carvalho, J. O., Potter, G. G., Thames, A., Zelinski, E., Crane, P. K., … Alzheimer's Disease Neuroimaging Initiative. (2012). The Alzheimer's Disease Assessment Scale-Cognitive-Plus (ADAS-Cog-Plus): An expansion of the ADAS-Cog to improve responsiveness in MCI. *Brain Imaging and Behavior*, *6*(4), 489–501. https://doi.org/10.1007/s11682-012-9166-3

Small, S. A., & Duff, K. (2008). Linking Aβ and tau in late-onset Alzheimer's disease: A dual pathway hypothesis. *Neuron*, *60*(4), 534–542.

Sperling, R. A., Mormino, E. C., Schultz, A. P., Betensky, R. A., Papp, K. V., Amariglio, R. E., … Hedden, T. (2019). The impact of amyloid-beta and tau on prospective cognitive decline in older individuals. *Annals of Neurology*, *85*(2), 181–193.

Stöhr, J., Watts, J. C., Mensinger, Z. L., Oehler, A., Grillo, S. K., DeArmond, S. J., … Giles, K. (2012). Purified and synthetic Alzheimer's amyloid beta (Aβ) prions. *Proceedings of the National Academy of Sciences of the United States of America*, *109*(27), 11025–11030.

Thal, D. R., Rub, U., Orantes, M., & Braak, H. (2002). Phases of A beta-deposition in the human brain and its relevance for the development of AD. *Neurology*, *58*(12), 1791–1800. https://doi.org/10.1212/wnl.58.12.1791

van Rossum, I. A., Visser, P. J., Knol, D. L., van der Flier, W. M., Teunissen, C. E., Barkhof, F., … Scheltens, P. (2012). Injury markers but not amyloid markers are associated with rapid progression from mild cognitive impairment to dementia in Alzheimer's disease. *Journal of Alzheimer's Disease*, *29*(2), 319–327.

Vandenberghe, R., van Laere, K., Ivanoiu, A., Salmon, E., Bastin, C., Triau, E., … Korner, A. (2010). 18F-flutemetamol amyloid imaging in Alzheimer disease and mild cognitive impairment: A phase 2 trial. *Annals of Neurology*, *68*(3), 319–329.

Villemagne, V. L., Burnham, S., Bourgeat, P., Brown, B., Ellis, K. A., Salvado, O., … Maruff, P. (2013). Amyloid β deposition, neurodegeneration, and cognitive decline in sporadic Alzheimer's disease: A prospective cohort study. *The Lancet Neurology*, *12*(4), 357–367.

Walker, L. C., & Jucker, M. (2011). Amyloid by default. *Nature Neuroscience*, *14*(6), 669–670.

Wang, L., Benzinger, T. L., Su, Y., Christensen, J., Friedrichsen, K., Aldea, P., … Morris, J. C. (2016). Evaluation of tau imaging in staging Alzheimer disease and revealing interactions between β-amyloid and tauopathy. *JAMA Neurology*, *73*(9), 1070–1077.

Weiner, M. W., Veitch, D. P., Aisen, P. S., Beckett, L. A., Cairns, N. J., Green, R. C., … Alzheimer's Disease Neuroimaging Initiative. (2017). The Alzheimer's Disease Neuroimaging Initiative 3: Continued innovation for clinical trial improvement. *Alzheimer's & Dementia*, *13*(5), 561–571. https://doi.org/10.1016/j.jalz.2016.10.006

Whitwell, J. L., Graff-Radford, J., Tosakulwong, N., Weigand, S. D., Machulda, M. M., Senjem, M. L., … Drubach, D. A. (2018). Imaging correlations of tau, amyloid, metabolism, and atrophy in typical and atypical Alzheimer's disease. *Alzheimer's & Dementia*, *14*(8), 1005–1014.

Williamson, R., Usardi, A., Hanger, D. P., & Anderton, B. H. (2008). Membrane-bound β-amyloid oligomers are recruited into lipid rafts by a fyn-dependent mechanism. *The FASEB Journal*, *22*(5), 1552–1559.

Wong, D. F., Rosenberg, P. B., Zhou, Y., Kumar, A., Raymont, V., Ravert, H. T., … Ye, W. (2010). In vivo imaging of amyloid deposition in Alzheimer disease using the radioligand 18F-AV-45 (flobetapir F 18). *Journal of Nuclear Medicine*, *51*(6), 913–920.

SUPPORTING INFORMATION

Additional supporting information may be found online in the Supporting Information section at the end of this article.

How to cite this article: Kim C-M, Montal V, Diez I, Orwig W, Alzheimer's Disease Neuroimaging Initiative (ADNI), Sepulcre J. Network interdigitations of Tau and amyloid-beta deposits define cognitive levels in aging. *Hum Brain Mapp*. 2021;42:2990–3004. https://doi.org/10.1002/hbm.25350